Evaluation of Flow Parameters around Tracking Solar Collectors with Different Collector Geometry and Different Operation Conditions

Khalid Hameed Hussein
Engineering Affair Department, University of Baghdad/ Baghdad
kh.alazzawi60@yahoo.com

Received on: 19/2 /2013 & Accepted on: 26/11 /2013

ABSTRACT

In the current study, the flow parameters around the tracking solar collectors were evaluated. Different site conditions with different tracking solar collector's geometry are combined and investigated. Site conditions included different wind loading due to different angles of attack and wind velocity. Collector's geometry included dish collector, parabolic trough collector and Heliostat collector. The flow parameters are estimated numerically by using a suitable computational fluid dynamics (CFD) package (ANSYS FLUENT 14) to solve the governing equations and boundary conditions. The verification of numerical results was done by comparing the numerical results with experimental results of the case of parabolic trough solar collector. The results of wind loading on all types of collectors and flow characteristics at different operation conditions are obtained and compared.

Keywords: Pressure, Velocity, Angle of Attack, Finite Element, and Solar Collector.

دراسة ظروف الجريان حول المجمعات الشمسية التتابعية ذات اشكال هندسية مختلفة وعند ظروف تشغيل مختلفة

الخلاصة

في هذه الدراسة , تم دراسة ظروف الجريان حول المجمعات الشمسية بكافة اشكالها.درس البحث مختلف الظروف التشغيلية مع مختلف اشكال المجمعات الشمسية. الظروف التشغيلية اشتملت على احمال هوائية مختلفة ناتجة عن اختلاف زوايا هجوم الرياح واختلاف سرعة الهواء. اشكال المجمعات تضمنت الصحن الشمسي والمجمع بشكل قطع مكافئ والمرأة الدوارة العاكسة لاشعة الشمس. درس البحث ايجاد خصائص الجريان حول المجمعات الشمسية وذلك باستخدام برنامج حاسوبي لديناميك الموائع لحل معادلات الحركة والظروف الحدية(ANSYS FLUENT 14). تم اجراء اختبارات عملياًلحالة معينة لمقارنة النتائج والتحقق من صحة النتائج العددية. في مختلف ظروف الجريان لكل انواع المجمعات الشمسية.

INTRODUCTION

Tracking solar solar collectors are used to concentrate the sun light onto special receiver to heat the working fluid which is used then in electricity generation and other applications. Figure (1) shows some types of solar collectors.

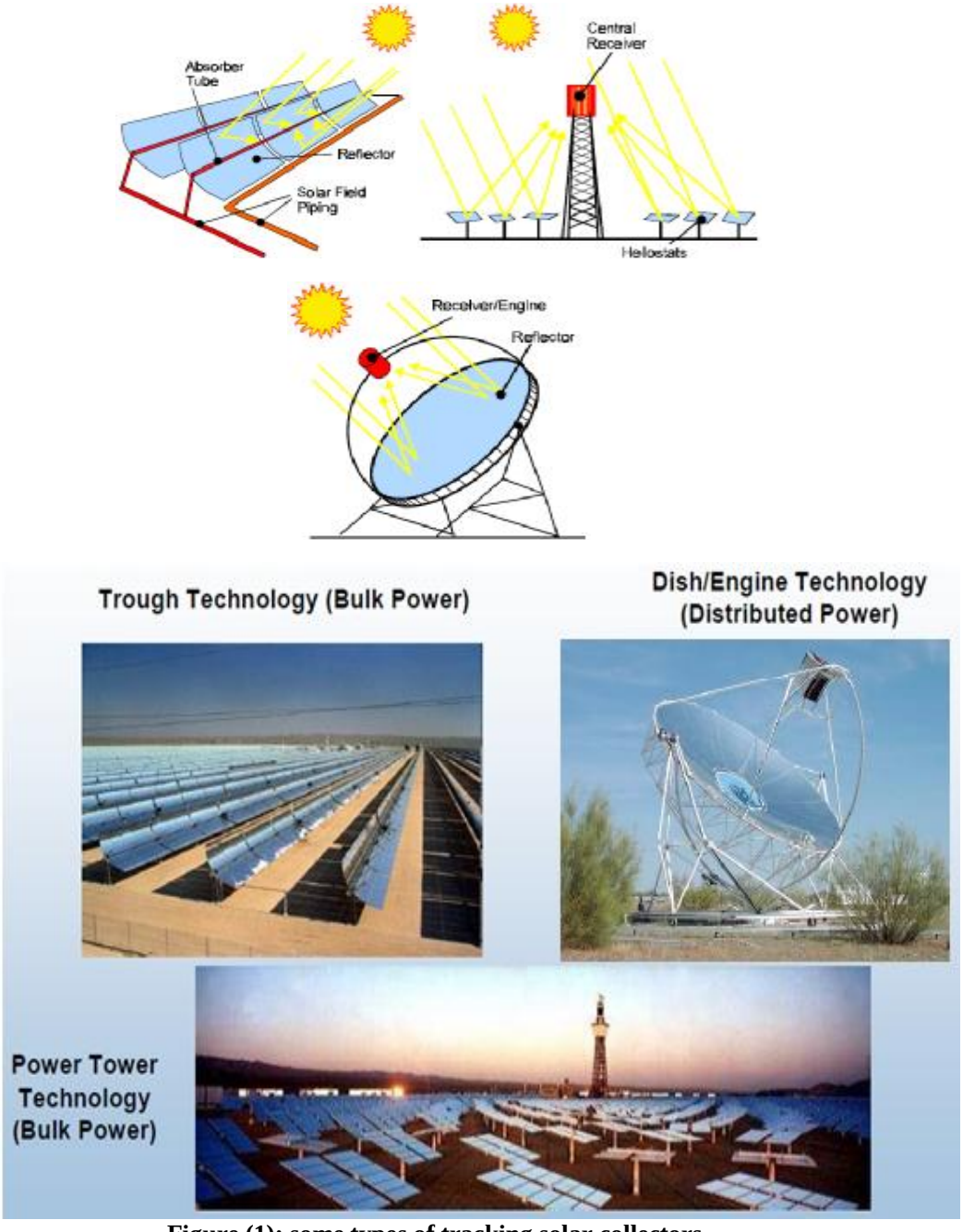

Figure (1): some types of tracking solar collectors.

The study of distribution of local pressure around the tracking solar collector is important task from the view point of mirror and support structure design. Also, solar thermal power plants are primarily installed in flat terrain of high solar irradiation for achieving a high power density **Soteris**[1]. At flat terrain, the components of plants are subjected to severe aerodynamic loading. The main environmental problems which affect the tracking solar collector performance are the wind-induced vibration and collector instability to truck the sun accurately **Naeeni and Yaghoubi [2]**. To overcome these problems, comprehensive solutions should be investigated. The key of these solutions is the comprehensive study of flow characteristic around the solar collectors **Hamad[3].** The estimation of all these parameter will give the base to introduce practical solutions for each aerodynamic problem. Pressures over the collector can vary in space and time, because of spatial and temporal variation in approach velocity (turbulence), the bluff geometry of the solar collector, and the wide range of the operational conditions. The studies on the effect of combination of the geometry and operation conditions on flow parameters around the solar collector are very rarely.

N. U. Gunasena[4]performs a study to determine the feasibility of a novel solar collector design for large scale solar power generation. The design concept involved a large, fixed mirror dish in the shape of a spherical segment, with a tracking collector as opposed to a more traditional tracking concentrator with a fixed or tracking collector. **J. A. Peterkaet. Al [5]**. carried out a study to define mean and peak wind loads on parabolic dish solar collectors. Loads on isolated collectors and on collectors within a fie1d of collectors were obtained. A major intent of the study was to define wind load reduction factors for collectors within a field resulting from protection offered by upwind co1lectors, wind protective fences, or other blockage elements. **N. Hosoya and J.A. Peterka [6]** carried out comprehensive experimental study to determine the mean and maximum wind load coefficients on the parabolic trough in boundary layer wind tunnel. The wind loading on parabolic trough are determined for different angles of attack, for different wind speeds and for different turbulent intensity. This study showed that the wind loads coefficients are independent of the Reynolds number and turbulent intensity. **A. Miliozzi et.al [7]**evaluates wind loads on a parabolic-trough concentrator numerically using the CFD Flotran module of Ansys finite element code. The study concentrated to evaluate the aerodynamics coefficient for the parabolic trough at three wind speed and different angular position.

In current study, the combination of the effects of the operation conditions and the geometry of solar collectors on flow parameters are investigated and compared with each other. The flow parameters includeddrag coefficient, lift coefficient, pressure distribution, velocity distribution, and vortex shedding. The types of tracking solar collectors are heliostat collector, dish collector and parabolic trough collector.

GOVERNING EQUATIONS:

The governing equations of fluid flow are

1- Conservation of mass (continuity equation)

$$\frac{\partial u}{\partial x}+\frac{\partial v}{\partial y}+\frac{\partial w}{\partial z}=0 \qquad \text{.....(1)}$$

Where u, v, and w are velocity components of fluid in x, y, and z directions.

2- Conservation of momentum (Navier–Stokes Equations)

in x- direction :

$$\frac{\partial P}{\partial x} + \rho\left(u\frac{\partial u}{\partial x} + v\frac{\partial u}{\partial y} + w\frac{\partial u}{\partial z}\right) = \rho g_x + \mu\left(\frac{\partial^2 u}{\partial x^2} + \frac{\partial^2 u}{\partial y^2} + \frac{\partial^2 u}{\partial z^2}\right) \quad \text{.....(2)}$$

in y- direction :

$$\frac{\partial P}{\partial y} + \rho\left(u\frac{\partial v}{\partial x} + v\frac{\partial v}{\partial y} + w\frac{\partial v}{\partial z}\right) = \rho g_y + \mu\left(\frac{\partial^2 v}{\partial x^2} + \frac{\partial^2 v}{\partial y^2} + \frac{\partial^2 v}{\partial z^2}\right) \quad \text{.....(3)}$$

in z- direction :

$$\frac{\partial P}{\partial z} + \rho\left(u\frac{\partial w}{\partial x} + v\frac{\partial w}{\partial y} + w\frac{\partial w}{\partial z}\right) = \rho g_z + \mu\left(\frac{\partial^2 w}{\partial x^2} + \frac{\partial^2 w}{\partial y^2} + \frac{\partial^2 w}{\partial z^2}\right) \quad \text{.....(4)}$$

Where p is the pressure, ρ is the fluid density, g is the acceleration and μ is the kinematic viscosity.

The governing equations in atmospheric boundary layer are Reynolds Averaged Navier-Stokes equations and RNG-based (Re-normalized Group)k-ε turbulent scheme**[8].**The Reynolds-averaged Navier-Stokes (RANS) equations govern the transport of the averaged flow quantities, with the whole range of the scales of turbulence being modelled. In RNG (k- ε) models, the turbulent kinetic energy is k and viscous dissipation rate of turbulent kinetic energy is (ε). The RNG turbulence model is more responsive to the effects of rapid changes and streamlines curvature, flow separation, reattachment and recirculation than the standard k-ε model and it has been used widely for wind flow studies **Yakhot** and **Orszag[9].**

BOUNDARY CONDITIONS

A power law boundary layer equation is used for the inlet boundary condition for the domain. The design wind speed is based on national wind load standard (ASCE 7-05) (American society of civil engineering). The modelled boundary layer profiles compare well with those suggested by ASCE 7-05 for winds over an open country exposure (α=0.14) and the turbulent boundary layer with 21% turbulence intensity. At the edges of domain, the symmetry boundary will apply. Symmetry boundary conditions are used when the physical geometry of interest and the expected pattern of the flow solution have mirror symmetry. Also the Symmetry boundaries are used to reduce the extent of computational model to a symmetric subsection of the overall physical system. The boundary condition at the collector's surface is wall with free slip conditions. Wall boundary conditions are used to bound fluid and solid regions. At the outlet, pressure outlet boundary condition was applied. Pressure outlet boundary conditions require the specification of a static (gauge) pressure at the outlet boundary. For the current simulation the outlet pressure equal to zero. The boundary conditions will be **[2]**

1- Inlet $u = 0.7244\, u_\infty\, z^{0.14}$ .....(5)

Where u_∞ is the wind velocity of 10m height and z is the height.

2- Exit $\frac{\partial p}{\partial x} = \frac{\partial u}{\partial x} = \frac{\partial v}{\partial x} = \frac{\partial w}{\partial x} = 0$ .....(6)

3- Wall

$$U^* = \frac{1}{k}\ln(Ez^*) \quad \text{.....(7)}$$

$$U^* = \frac{\rho U_p C_\mu^{1/4} k_p^{1/2}}{\tau_w} \quad \text{.....(8)}$$

$$Z^* = \frac{\rho C_\mu^{1/4} k_p^{1/2} z_p}{\mu} \quad \text{.....(9)}$$

Where

E: empirical constant(=9.81)
K: Von Karman constant (=0.42)
U_p: fluid velocity at any point p
C_μ: empirical constant
K_p : turbulence kinetic energy at any point p
τ_w: wall shear stress
z_p : distance from any point p to the wall.

NUMERICAL PROCEDUER

The numerical simulation steps consist of three steps as shown in Figure (2). The simulation began from preprocessing stage which included geometry setup, grid generation and boundary condition setup. The geometry of the model, the grid generation and boundary conditions setup was done by using software package (GAMBIT2.4.6.). After that, the complete model (geometry and mesh) was exported from GAMBIT 2.4.6) to the (ANSYS FLUENT) software. The second stage was the computational simulation which done by using software package(ANSYS FLUENT) solver. Finally is the post-processing stage where the aerodynamics characteristics(results) were found. The geometry of tracking solar collectors is shown in figure (3).

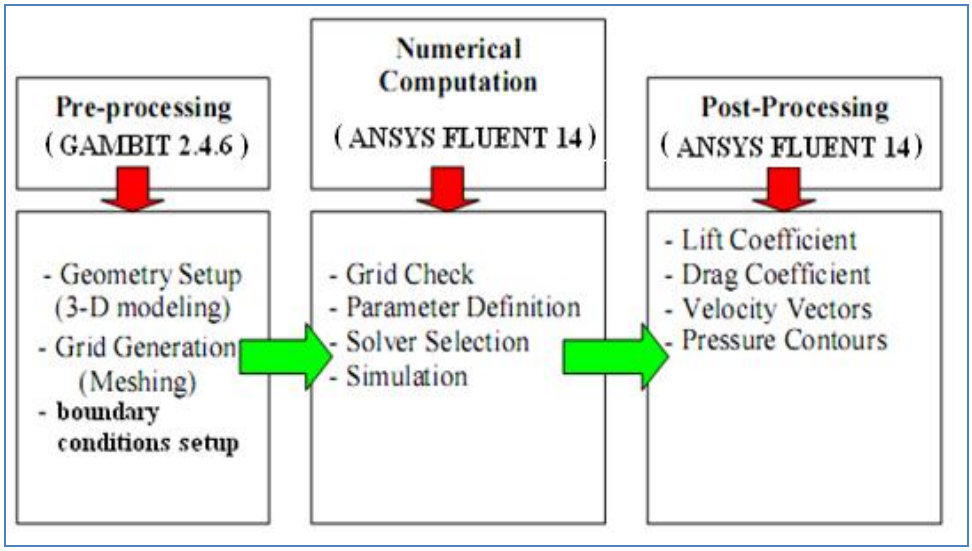

Figure (2): Stages of Numerical simulation

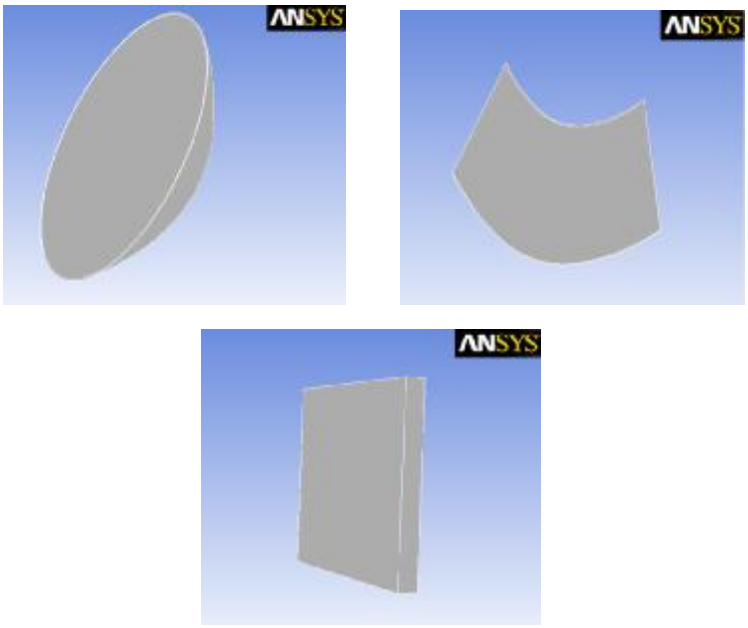

Figure (3): Geometry of solar collectors.

The unstructured tetrahedral mesh was used for simulating the flow around the model. In unstructured approach, the integral form of governing equations is discretized and either a finite-volume or finite-element scheme is used. Unstructured grids are in general successful for complex geometries **Hanaa [10].**Volume mesh can be created using T-grid, Gambit scheme. Size functions are used to control the size of mesh interval for edges and mesh elements for faces or volumes and thus to keep

smooth transition of mesh from fine mesh near the trough faces to coarse mesh far away at the undistributed boundaries. After the meshing process, themesh was checked. It was to check on the quality of the mesh by observing the skewness level and abrupt changes in cell sizes as shown in Figure (4).

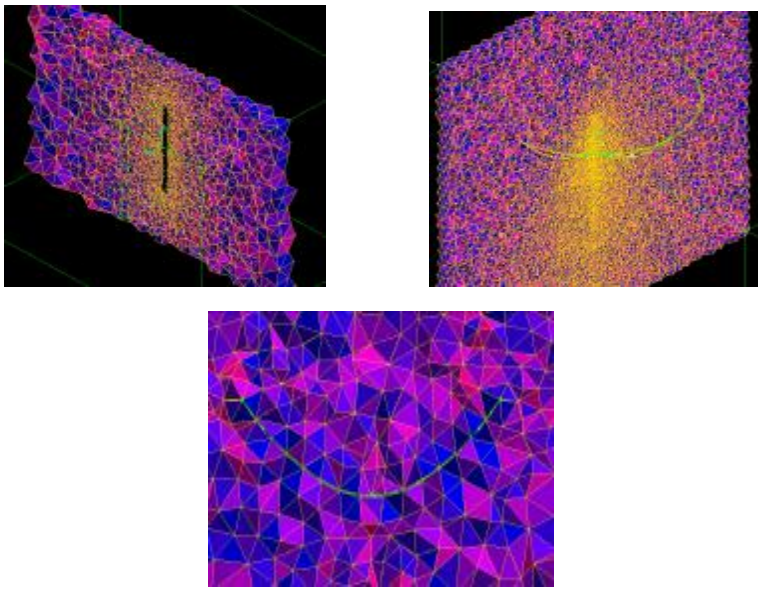

Figure (4): Mesh distribution around the solar collectors

The numerical simulation by Fluent 14 was made after the mesh generation. The solver formulation, turbulence model, boundary condition, solution control parameters and material properties were defined. Table (1) lists the numerical simulation steps and appendix 1 illustrates these steps. After all the parameters were specified, the model was initialized. The initializing and iteration processes stopped after the completion of the computations. The results obtained were examined and analyzed.

Table 1: Numerical simulation steps

step	Task	Details
1	Importing the model from GAMBIT 2.4.6	file→read→Mesh→(saved mesh)
2	Turbulence model establishment	Model→Viscos-laminar→K-epsilon→RNG
3	Material specification	Material→Air→(density and viscosity)
4	Boundary conditions specification	Boundary condition→inlet(velocity value) and outlet(zero pressure)
5	Solution method parameters	Solution methods→scheme(simple), Gradient (least squares), pressure(second order) and momentum(second order)
6	Results	Velocity contours, pressure contours, drag value, lift value, moment value

DIMENSIONS OF PROTOTYPES:

The determination of wind loading and flow characteristics around the solar collectors and the comparison between these results requires that the projected area leeward the wind attack for all types of solar collectors are the same. To achieve this goal, the dimensions of each collector should be modified for each angle of attack. At beginning, the projected area of dish collector is computed by using fluent. Then the length of trough collector and plate collector was modified to get the same projected area. This procedure is repeated for each angle of attack for drag calculation, for lift calculation, for pressure distribution and for velocity distribution.

OPERATION CONDITIONS:

The solar collector tracks the sun along the working day to concentrate the sun light onto working fluid. Therefore, the orientation of solar collector changes continuously along the day. So, the angles of attack of wind with collector will also changes along the day. Many angles of attack of wind with collector were investigated. These angles of attack (θ) are (0°, $+15^\circ$, $+30^\circ$, $+45^\circ$, $+60^\circ$, $+75^\circ$ and $+90^\circ$) where at ($\theta=0^\circ$) the aperture of collector is parallel to wind direction and at ($\theta=90^\circ$) the aperture is normal to wind direction. Also, the wind speed changes continuously. Therefore different wind speeds are examined. The wind speed range were examined is (5, 7.5,10, 12.5, 15m/s).

RESULTS AND DISCUSSIONS:

The results of current study will divided into many sections. The first section concerns with the verification of numerical results by comparing the results of numerical simulation of parabolic trough with the experimental results of the same case. The second section presents and discusses the results of flow distributions around the each type of collector at different site conditions. The next section presents and discusses of wind loading (drag and lift) on each type of collector at different site conditions. The aim of study is to determine the perfect operation conditions of each type of collector and determine which collector is more suitable at specific operation conditions.

VERIFICATIONS OF NUMERICAL RESULTS:

Figure**s** (5 and 6) show the pressure distribution around the parabolic trough at wind velocity (15m/s) and angle of attack (90°) obtained from experimental work and numerical simulation respectively. The experimental data are performed in boundary layer wind tunnel tests in national renewable energy laboratory **Hosoya and Peterka[6].** The comparison between experimental and numerical results show good agreement and gives the validity for numerical simulation to estimate the flow characteristics around the same structure at identical flow boundary conditions. The comparison between these figures shows the same gradient of values of pressure from plus value near the bottom edge and at middle the collector to minus value (vacuum pressure) near the top edge. Also, it is observed that there is longitudinal gradient in pressure values near the edges. This means that the points which lie on the same longitudinal line have the close value of pressure. This observation was noted from both numerical simulation and experimental work. The other verification between the numerical simulation and experimental is the value of local distributed pressure where the values which obtained from numerical simulation are close to that obtained

from experimental work. Table 2 shows comparison between these values at some points (shown in figure 5) on trough surface and the percentage of error.

Table 2: Comparison between experimental and numerical results of pressure

point	Pressure value(bar) (experimental)	Pressure value(bar) (numerical)	Error percentage
1	1.4	1.51	7.28%
2	1	0.887	-12. 739%
3	-1.6	-1.5	6.667%

Figure (5): pressure distribution over trough surface obtained from experimental work (bar) [6].

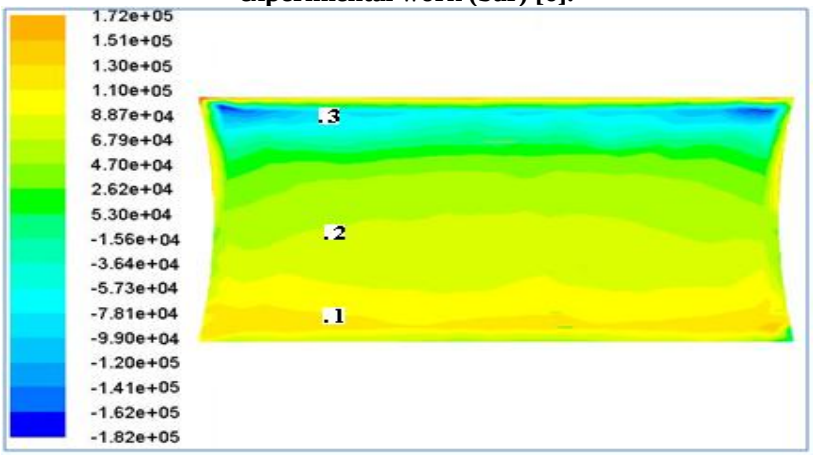

Figure (6): pressure distribution over trough surface obtained from numerical simulation (Pascal).

FLOW DISTRIBUTION RESULTS:

The flow characteristics included pressure distribution, velocity distribution and turbulence distribution. Figure (7) shows the pressure distribution over the surface of the solar collectors at wind velocity 15m/s and angle of attack (θ=90˚).It is clear from this figure that the dish and trough collectors expose to high gradient of pressure over its surface. This gradient can be attributed to the effect of curvature of the collector. The curvature of the dish and trough lead to complex behavior of fluid around the collector due to separation, reattachment and vortex shedding.

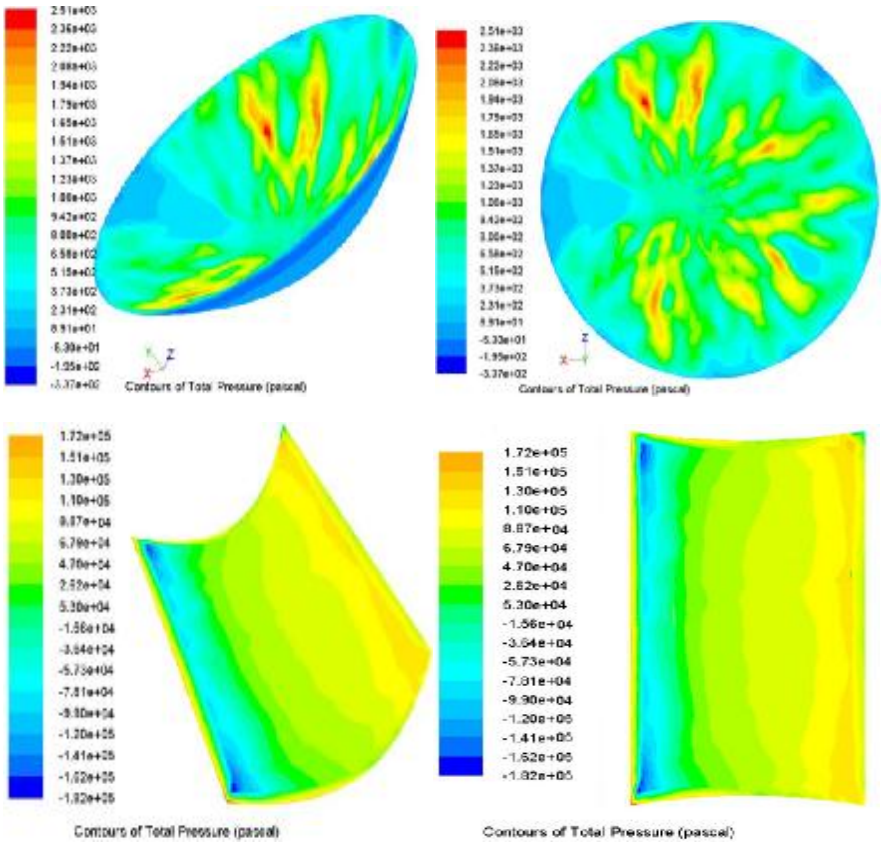

To be continued Fig. (7)

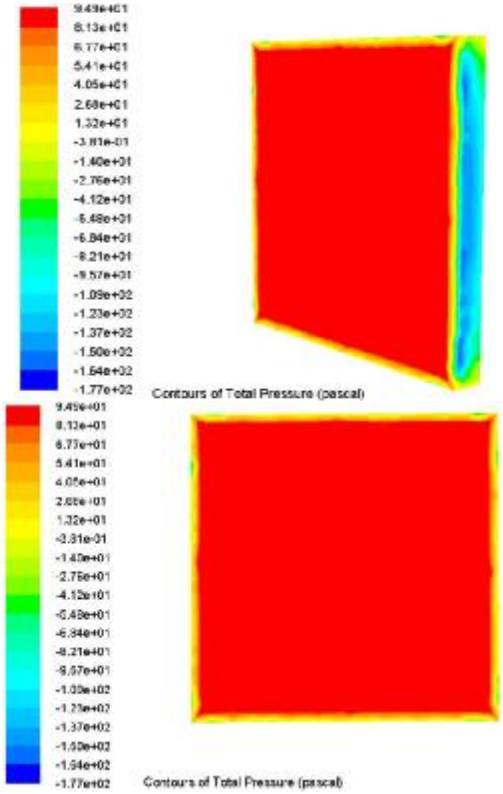

Figure (7): Isometric and front view of contours of pressure around the all types of solar collectors.

The gradient of pressure around the dish collector is more than that around the trough collector. This gradient leads to more considerations in mirror design to withstand the wind dynamic loads. The fluctuating wind loading on mirror structure leads to dynamic response. This response includes displacement, velocity, acceleration, stress, and strain. This response leads to degradation in collector performance and may to failure if the load and response exceeds the elastic limit of the structure. Also the fluctuating loads leads to dynamic response (dynamic stress) which may be leads to fatigue and fracture failure.

Figure (8) shows the turbulence intensity distribution around the mid section of all types of collectors. It is obvious that the high turbulence intensity occurs near the edges of heliostat and trough collectors. The turbulence around the dish collector is less than that around the trough collector. The high level of turbulence around the collector encourages the collector to exhibit dynamic response and subsequently a remarkable decreasing in collector performance will induced. The high level of turbulence located near the edges of collectors belongs to the effect of vortex shedding near the edges of collectors. This estimation about the turbulence encourages the using of dish collector more than the trough and heliostat collectors.

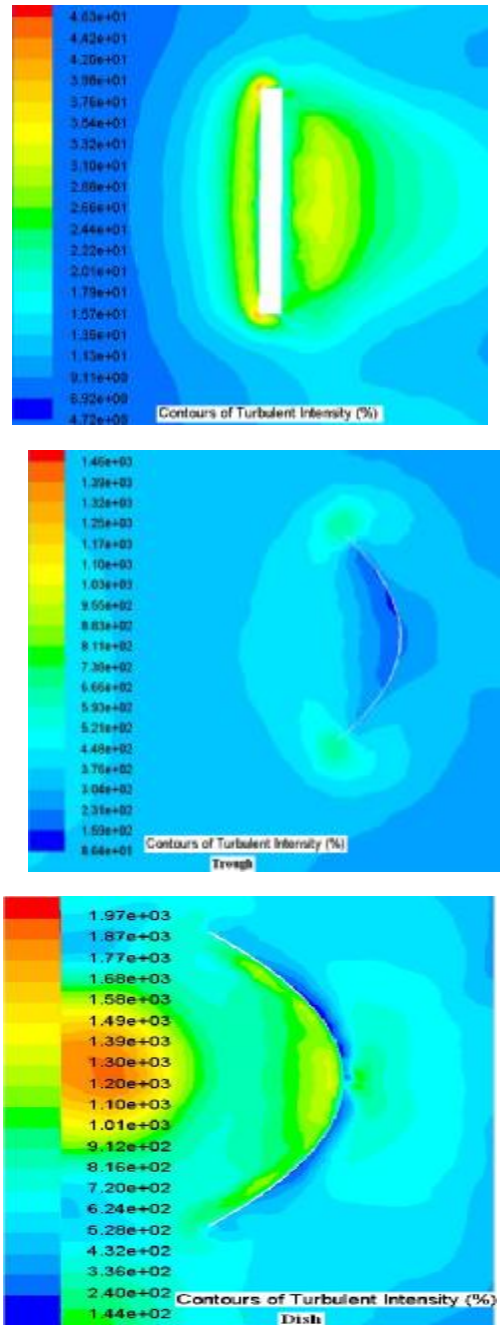

Figure (8): Turbulence distribution around the collectors at wind velocity 15m/s and angle of attack 90˚.

Also, the effect of velocity of wind and angle of attack on pressure distribution and turbulence intensity was estimated. The increasing of wind velocity leads to increase the pressure distribution over the collectors. It is shown from

numerical simulation that the increasing of wind velocity leads to increasing the pressure values over the dish collector surface more than the trough collector and the trough collector more than the heliostat collector. Figure (9) shows the average percentage of pressure increasing on collector types versus the increasing of wind velocity. The percentage of increasing are calculated where the base value of pressure are taken at wind velocity 3m/s and. The values of increments in pressure at 30 point on collectors surfaces are taken into account and the average value are calculated. Also, the increasing of wind velocity causes the increasing of turbulence intensity of trough collectors more than the heliostat and the heliostat more than the dish collector. Figure (10) shows the average value of percentage of increasing in turbulence intensity over the collectors surfaces versus the increasing of wind velocity where the base value of turbulence at 3 m/s. So, from the view point of pressure effect, the dish collectors is more sensitive to velocity changes and from the view of turbulence effect, the trough collector is more sensitive to velocity changes. Also, the changes of angle of attach at constant wind velocity leads to changes of pressure and turbulence distribution. The changing of angle of attack from 0˚ to 90˚ leads to remarkable increments in pressure values over the collector's surface. These increments observed for dish collector higher than that of trough and heliostat. The same situation was observed for the turbulence intensity. This increasing in pressure value and turbulence intensity caused because that the collectors expose severe aerodynamic conditions when the aperture of collector was normal to wind attack. The figures (11 and 12) show the average value of pressure and turbulence increasing percentage versus the angles of attack. The percentage of increasing of both pressure and turbulence are calculated from base value at angle of attack (0˚) and the increments at 30 points over collector surface are used to calculate the average value.

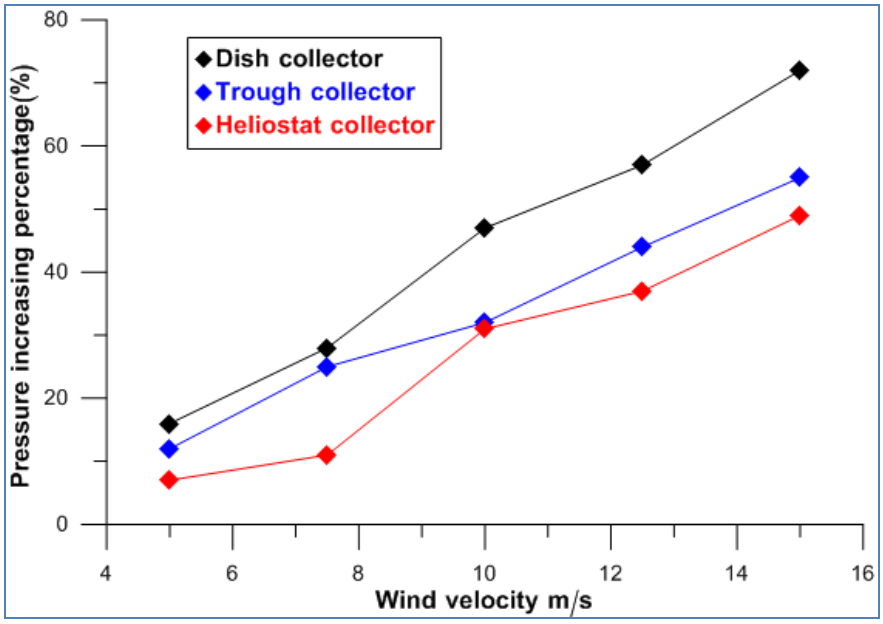

Figure (9): Pressure increasing percentage versus the wind velocity.

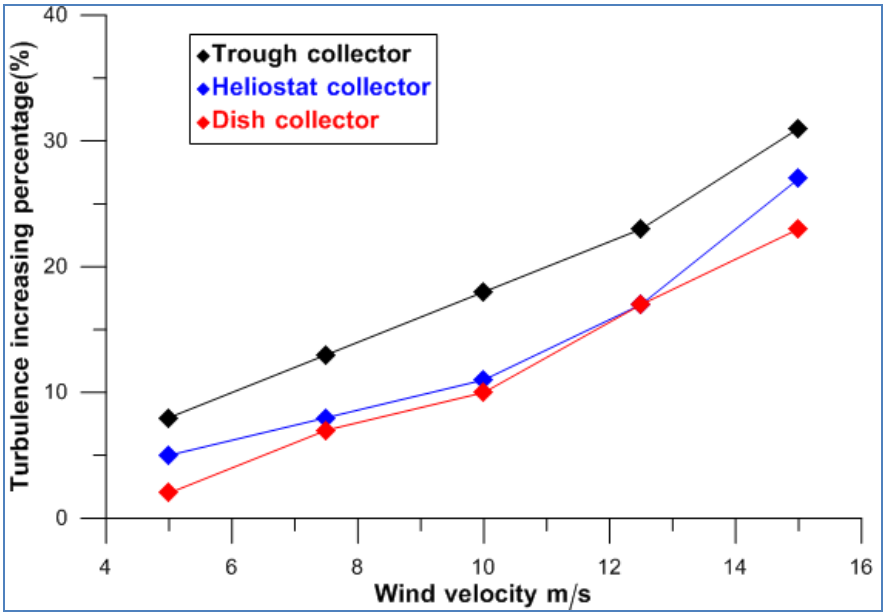

Figure (10): Turbulence intensity increasing percentage versus the wind velocity.

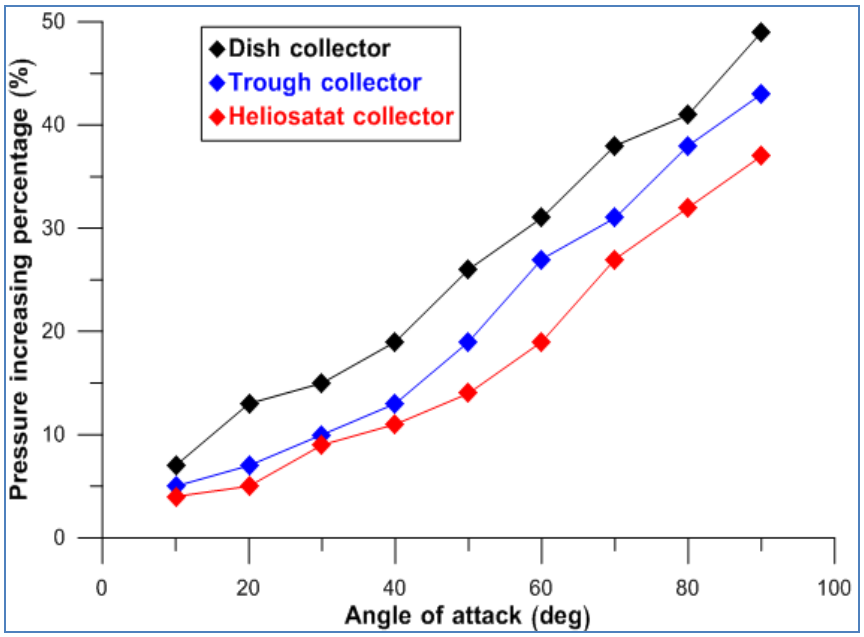

Figure (11): pressure increasing percentage versus angle of attack.

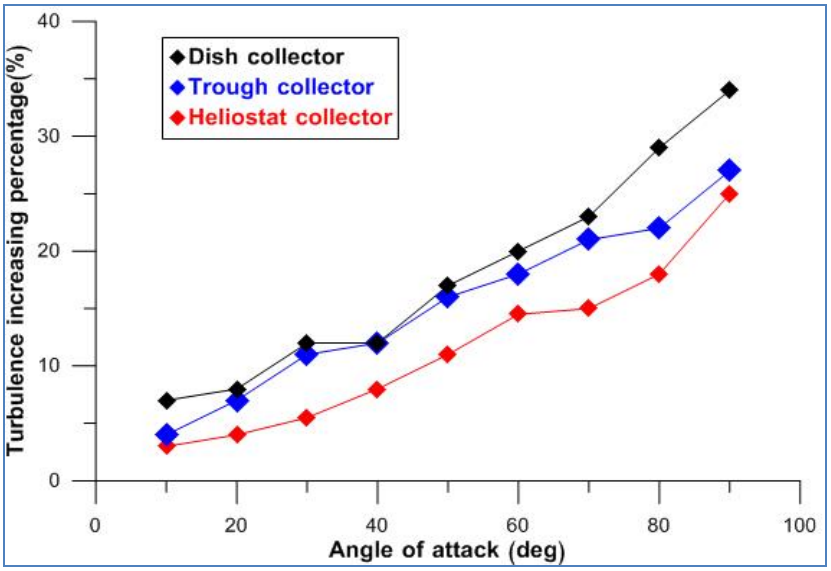

Figure (12): Turbulence intensity increasing percentage versus angle of attack.

The final observation on flow characteristics that the formation of many recirculation regions near the edges of the collectors. The size of these regions increases when the wind velocity increases. Also, the number and pattern of formation of these regions changes with the angle of attack. The severe aerodynamics conditions leads to more recirculation and vortex shedding. So, the changing of angle of attack from angle of attack 0˚to 90˚ leads to more recirculation and vortex shedding formation. Figure (13) show typical velocity counters around the tracking solar collectors.

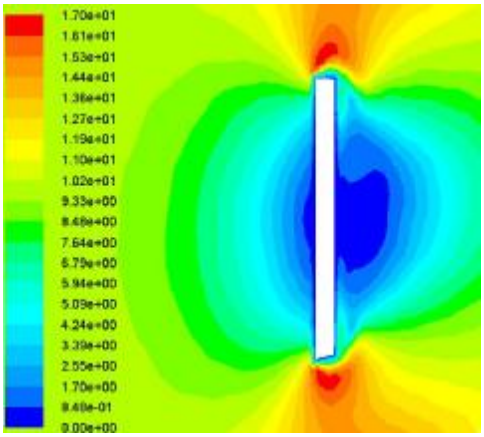

To be continued Fig. (13)

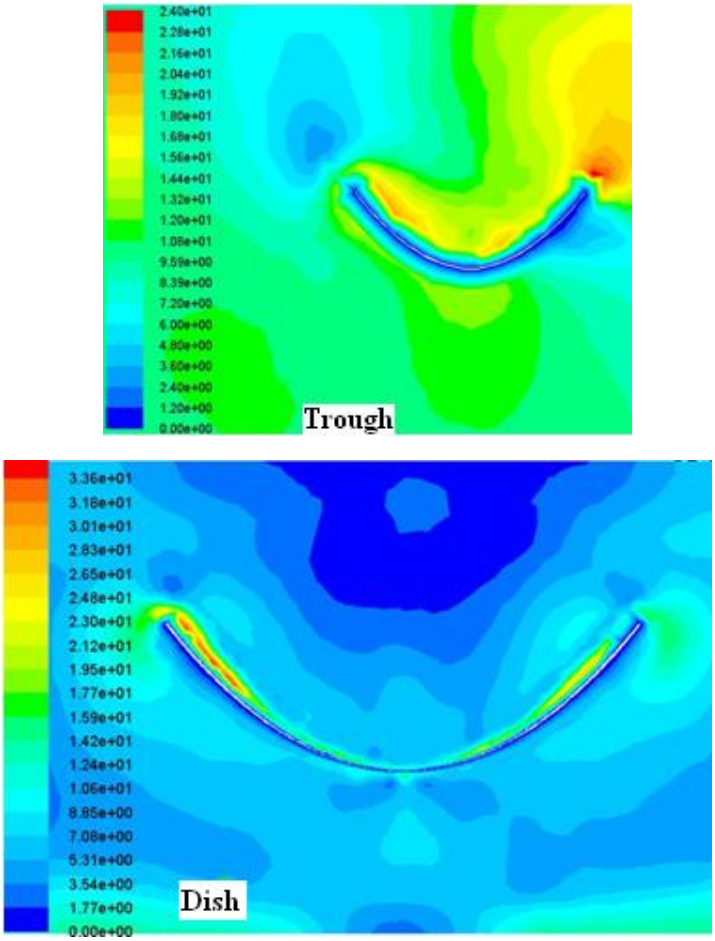

Figure (13): Velocity distribution contours around the collectors.

WIND LOADING (DRAG AND LIFT) RESULTS:

Figure (14) shows the results of wind loading coefficients on all types of tracking solar collectors obtained from numerical simulation. The first general observation from these results that the increasing of wind velocity has different effects on wind loading of the types of tracking solar collectors as seen in figure (14). For heliostat and parabolic trough, the change of wind velocity does not lead to remarkable changes in wind loading coefficients values. The values of wind loading coefficients for different wind velocity are close to each other and their order was changed at each angle of attack. For example, the value of drag coefficient of heliostat at angle of attack (30˚) and wind velocity 10m/s is higher than that at wind velocity 5m/s but this situation was reverse at angle of attack (45˚). For parabolic dish tracking solar collector, there is a regular and slight increasing in drag and lift coefficient value with the increasing of wind velocity. Among these three types, a parabolic dish seems to be more sensitive to change wind velocity. This can be attributed to the geometrical effects. More curved edges leads to more sensitivity for the changes in wind velocity. The second observation is that all types of tracking

solar collectors have the same trend of change of wind loading coefficient with angle of attack. The drag coefficient increases with the increasing of angle of attack within the range in current study for all types of collectors. The drag coefficient began at high value at (θ=0˚) and decreases to lowest value at angle of attack near 40˚ and then increases to highest value. This trend of change of lift force is observed for all types of collectors. The next observation that the values of wind load coefficients of parabolic trough collector was higher than that of heliostat and parabolic dish at the same angle of attack and wind velocity. The last observation is that there is an invert in the direction of lift coefficient of parabolic dish collector near angle of attack (θ=70˚). This invert was noted for parabolic dish only within the range of angle of attack considered in current study.

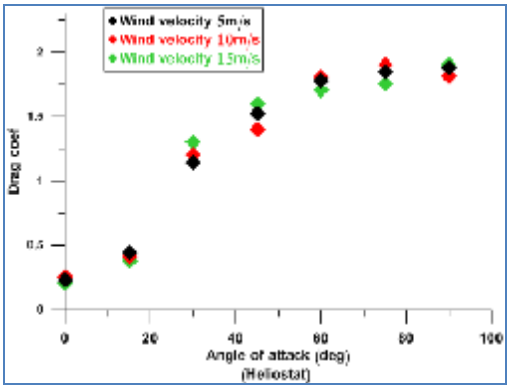

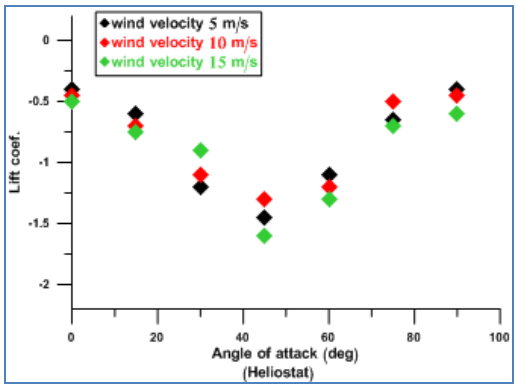

To be continued Fig. (14)

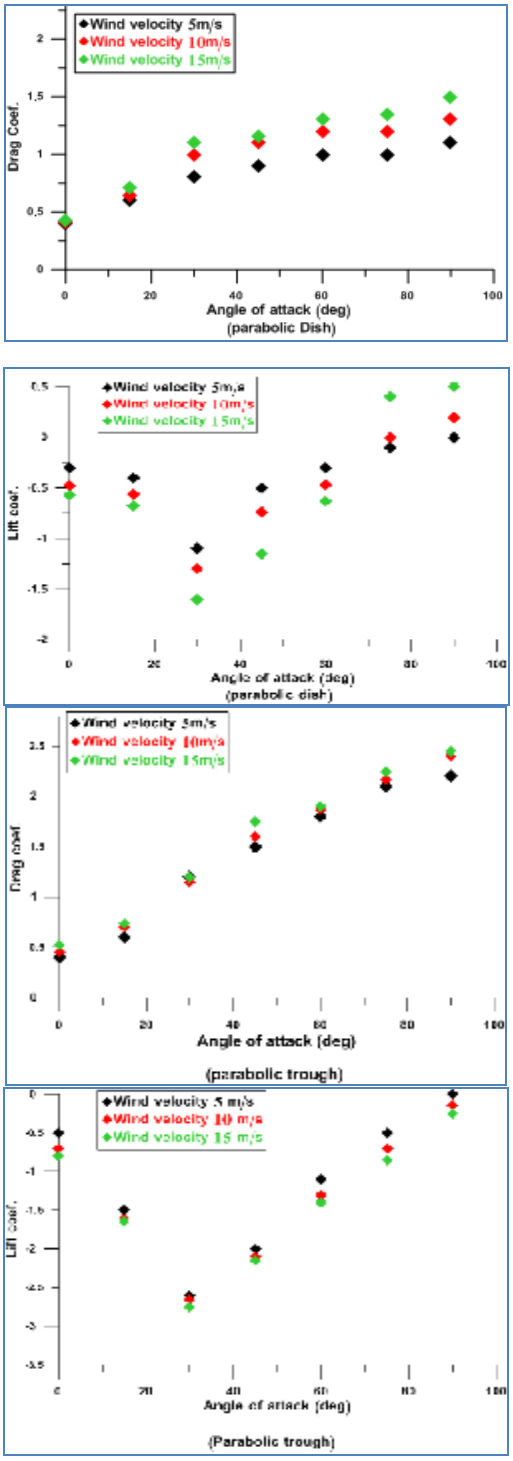

Figure (14): Wind load coefficients of all types of tracking solar collectors.

CONCLUSION:

1-Among these three types of collector, a parabolic dish seems to be more sensitive to change of wind velocity.
2- The values of wind load coefficients of parabolic trough collector was higher than that of heliostat and parabolic dish at the same angle of attack and wind velocity.
3- The gradient of pressure around the dish collector is more than that around the trough collector and heliostat collector.
4- The turbulence around the dish collector is less than that around the trough collector.
5- The increasing of wind velocity leads to increasing the pressure values over the dish collector surface more than the trough collector and the trough collector more than the heliostat collector.
6- The increasing of wind velocity causes the increasing of turbulence intensity of trough collectors more than the heliostat and the heliostat more than the dish collector.
7- The changing of angle of attack from 0˚ to 90˚ leads to remarkable increments in pressure values over the collector's surface. These increments observed for dish collector higher than that of trough and heliostat.

REFERENCES:

[1] Soteris A. Kalogirou" Solar thermal collectors and applications" Progress in Energy and Combustion Science, 30 (2004), 231–295.
[2] N. Naeeni, M. Yaghoubi, “Analysis of wind flow around a parabolic collector” Renewable Energy 32 (2007) 1898–1916.
[3] H. H. Hamad, "study on the dynamic response of solar concentrating power system", Ph.D thesis, University of technology, Mechanical Engineering Dept., 2012.
[4] N. U. Gunasena, “An experimental study of mean wind forces on hemispherical solar collectors”, M.Sc thesis, Texas tech university, 1989.
[5] J.A.peterka, Z. Tan, B. Bienkiwicz, J. E. Cermak, Fort Collins, “Wind Loads on Heliostatsand Parabolic DishCollectors”, Solar energy research institute, 1988.
[6] N. Hosoya and J.A. Peterka,” wind tunnel tests of parabolic trough solar collector”, National renewable energy laboratory, 2008.
[7] A. Miliozzi, D. Nicolini, G. Arsuffi and L. Sipione. Numerical evaluation of Wind action on Parabolic Trough Collectors.8th. World Congress on Computational Mechanics (WCCM8). 2008.
[8] Ansys fluent reference theory. Twelve edition, 2009.
[9] Yakhot V, OrszagSA, "Renormalization group analysis of turbulence", Journal of Science and Computational 1986.
[10] Hanaa A. H. “Numerical and Experimental investigation on the effect of restriction shape on characteristics of airflow in a square duct” PH.D thesis,Mech. Eng. Dept., Univ. Of Technology, 2006.

Appendix 1: interfaces of software (fluent) setup

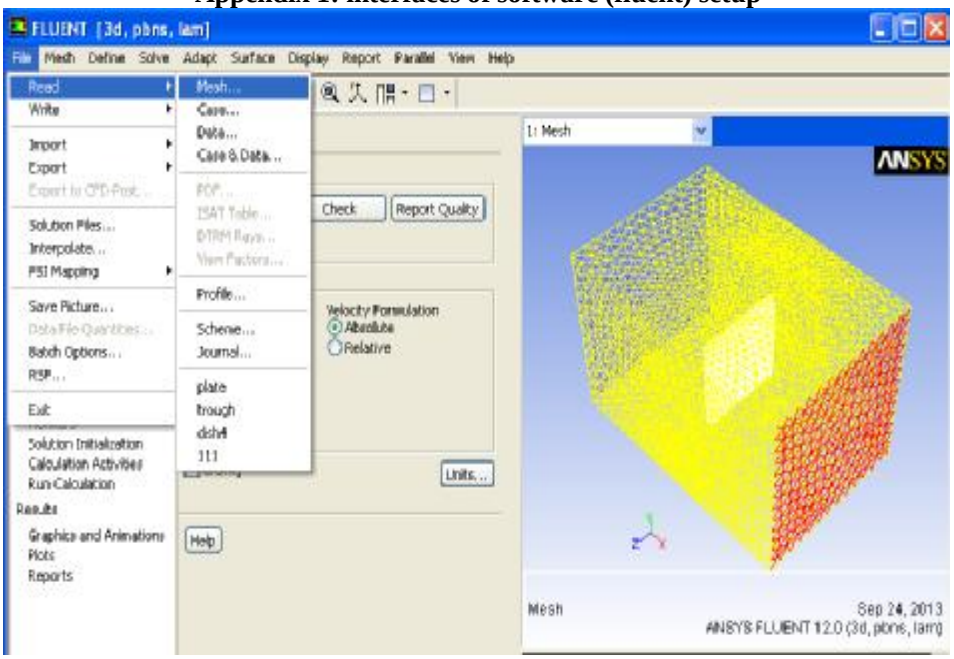

Fig 1: importing the model from gambit scheme

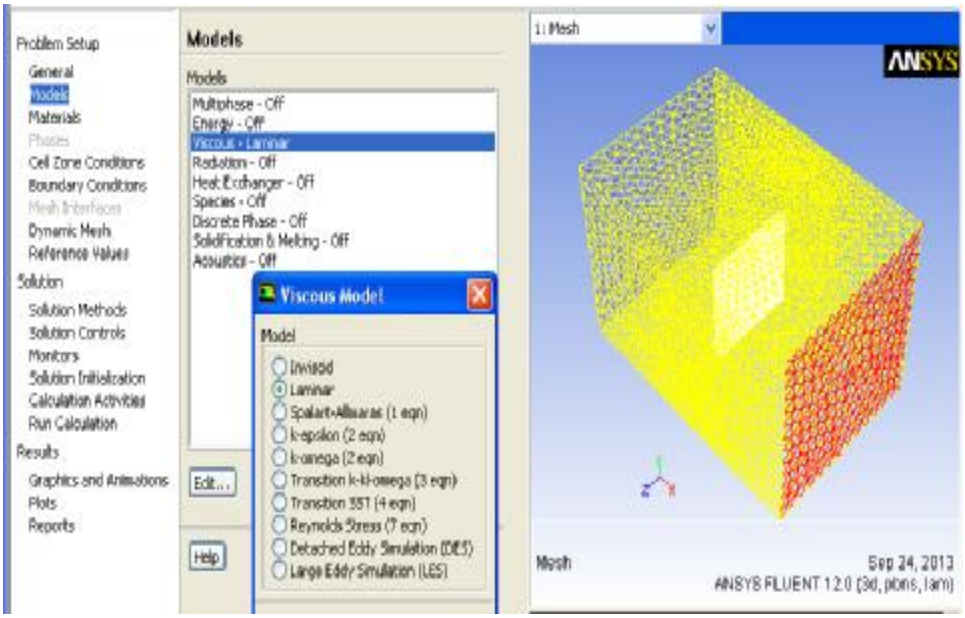

Fig 2: turbulence model setup

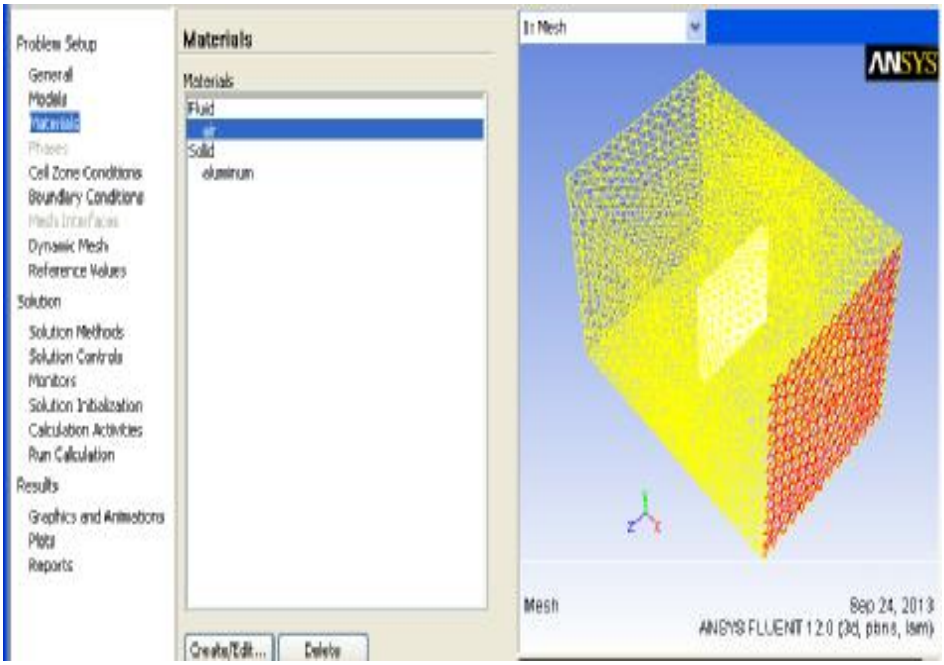

Fig 3: material properties setup

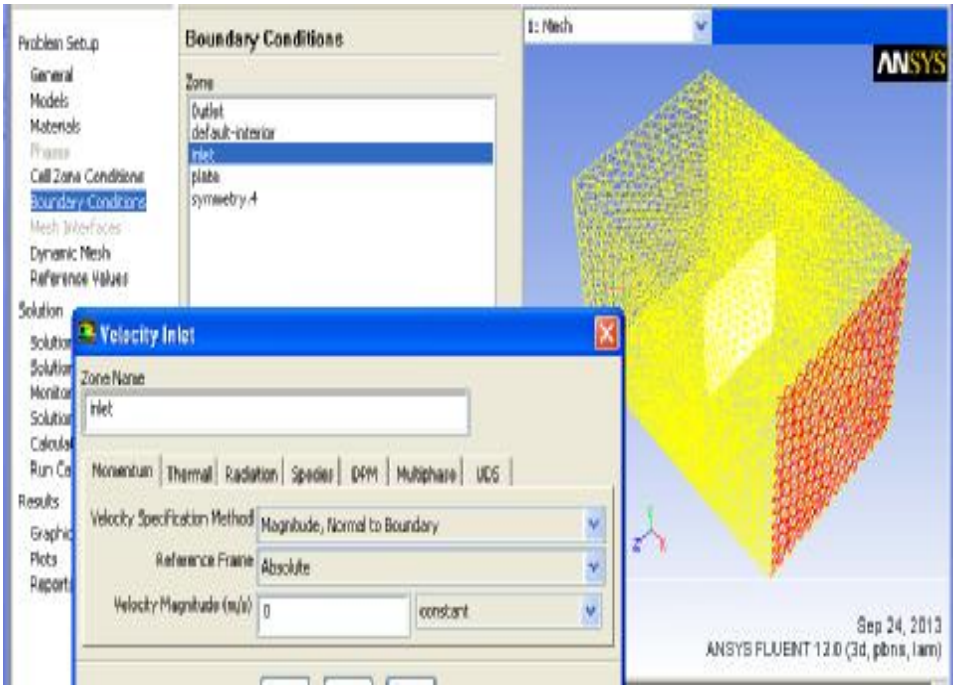

Fig 4: boundary condition setup

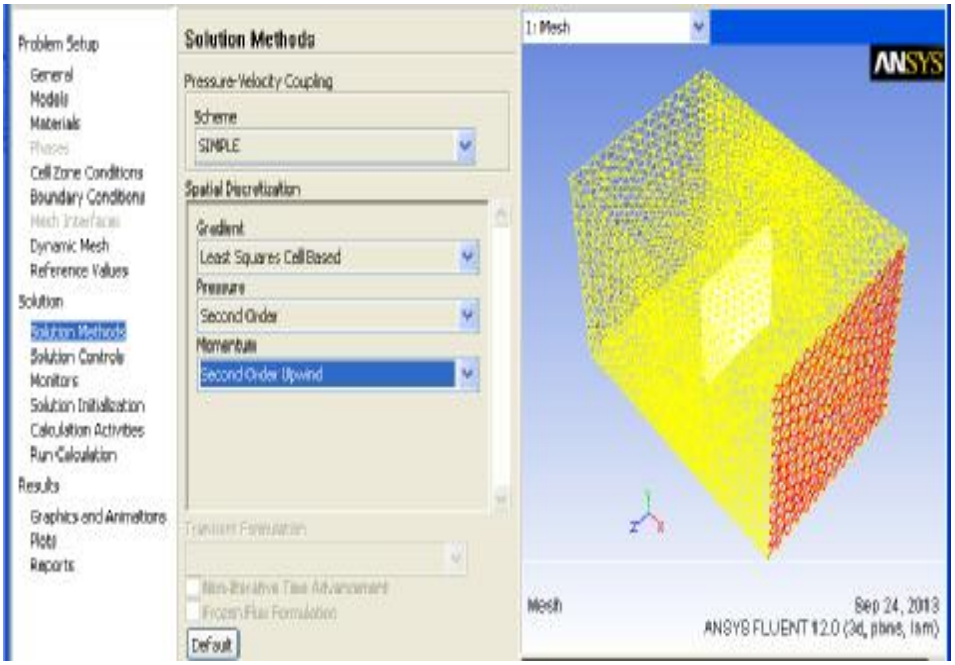

Fig 5: solution methods setup